UC Berkeley
UC Berkeley Previously Published Works

Title

Aqueous-Processable Redox-Active Supramolecular Polymer Binders for Advanced Lithium/Sulfur Cells

Permalink

https://escholarship.org/uc/item/11z3209x

Journal

Chemistry of Materials, 30(3)

ISSN

0897-4756

Authors

Hwa, Yoon
Frischmann, Peter D
Helms, Brett A
et al.

Publication Date

2018-02-13

DOI

10.1021/acs.chemmater.7b03870

Peer reviewed

Aqueous-Processable Redox-Active Supramolecular Polymer Binders for Advanced Lithium/Sulfur Cells.

Yoon Hwa[§,∫], Peter D. Frischmann[Σ], Brett Helms[Σ,†,*], Elton J. Cairns [§,∫,*]

§ Energy Storage and Distributed Resources Division, Lawrence Berkeley National Laboratory, One Cyclotron Rd., Berkeley, California, 94720, USA

∫ Department of Chemical and Biomolecular Engineering, University of California, Berkeley, California, 94720, USA

Σ The Joint Center for Energy Storage Research, Lawrence Berkeley National Laboratory, One Cyclotron Rd., Berkeley, California, 94720, USA

† The Molecular Foundry, Lawrence Berkeley National Laboratory, One Cyclotron Rd., Berkeley, California, 94720, USA

ABSTRACT: Lithium/Sulfur (Li/S) cells are a promising chemistry with potential to deliver a step-change in energy density compared to state-of-the-art Li-ion batteries. To minimize the environmental impact of the Li/S cell manufacturing and to compete with Li-ion cells in both performance and cost, electrodes cast using an aqueous process are highly desirable. Here we describe the discovery and application of a lithiated redox-mediating supramolecular binder based on the well-known n-type semiconductor, perylene bisimide, that forms high-fidelity sulfur electrodes from water-processed slurries. A 1.4-fold improvement in sulfur utilization at 3.0 C and 58 % increase in capacity retention after 250 cycles at 1.5 C are reported for the pre-lithiated, supramolecular binder compared to control samples. These improvements are attributed to the self-assembly of lithiated perylene bisimide binders in water to yield nanowire web morphologies that increase interfacial area between electrode components and exhibit enhanced electrode-current collector adhesion.

INTRODUCTION

Li-ion batteries are approaching a fundamental performance plateau that fails to meet the future needs for fully electric-powered human mobility. Accelerated development of alternative, next-generation battery chemistries that can deliver high specific energy and power density is critical to enabling emerging markets like electric-powered flight and long-haul trucking. In addition to high practical specific energy > 400 Wh/kg, commodity energy storage systems for transportation applications must be manufactured at a competitive price approaching \$100/kWh. Undoubtedly, an ambient temperature lithium/sulfur (Li/S) cell is regarded as one of the most promising next-generation energy storage systems due to its high theoretical specific energy of 2600 Wh/kg (vs. ~ 600 Wh/kg for conventional Li-ion), the low cost of S (< \$200/ton), the low environmental impact of S, and the improved safety of the cell.[1-4]

However, several challenges associated with the S electrode need to be overcome before a practical Li/S cell may compete with Li-ion chemistry for commercial dominance: the poor electrical conductivity of S and Li2S;

an 80% volume expansion of S particles upon lithiation; and lithium polysulfide dissolution into organic liquid electrolytes,[5,6] which results in low power/utilization and short cycle-life. To overcome these formidable challenges, a rational configuration of the Li/S cell is necessary with regard to all cell components such as the S electrode,[7-18] membrane (or interlayer),[19-21] electrolyte,[14, 22-24] and Li metal anode.[25] While a holistic approach to S electrode optimization is desirable, the majority of S electrode research has focused on developing high surface area conductive additives, polysulfide-blocking membranes, and polysulfide dissolution suppression systems[7-18]—functional binder development has thus far been underrepresented.[26]

Recently, we demonstrated multi-functional π-stacked perylene bisimide (PBI)-based redox-active binders undergo electrochemical reduction and lithiation in situ (i.e., PBI + 2e[-] + 2Li[+] ⇌ Li$_2$PBI), and in turn improve S utilization at high rate.[27] The proximity of Li$_2$PBI to S active materials significantly reduces cell impedance and maintains stable cycling performance. Moreover, unexpected synergies between Li$_2$PBI and a conventional polyvinylidene difluoride (PVDF) binder were discovered that further improved the electrochemical performance of the S electrode. Interestingly, these redox-active binders are not traditional high molecular-weight polymers, but rather supramolecular polymer binders consisting of molecular sub-units of PBI, a well-known n-type semiconductor with a long history in organic electronics.[28] This supramolecular approach to binder design affords more intimate mixing in the slurry of electrode components and offers potential for reconfigurabiltiy as the S active material expands and contracts. Expanding the development of multi-functional supramolecular binders represents a new pathway of research to mitigate the drawbacks of the S electrode. It remains a challenge to control the nanostructure of redox-mediating binders in a composite cathode with respect to the interface area between the mediator network, S, and conductive carbon; obviating the use of additional high-polymer binders (e.g., PVDF) in the cathode formulation is also desirable.

Here we report a new redox-active supramolecular polymer binder engineered for aqueous processing by chemical pre-lithiation of PBI (**1 +4LiOH ⇌ Li$_4$1**, Figure 1a), toward maximizing the environmental and cost benefits of Li/S cells. Although several organic solvents, especially N-methyl-2-pyrrolidone (NMP), are suitable for slurry formulation and electrode casting, they integrated in the manufacturing line. As S is chemically stable in water, a water based slurry is practical and very attractive.[29] The aqueous-processable, nano-structured supramolecular PBI binders reported here are also redox mediators, as previously reported in non-aqueous electrolyte,[30-32] activated by electrochemical reduction in operando at 2.5 V (vs. Li/Li[+]) during the first discharge, resulting in lithiation of the binder (**Li$_4$1 ⇌ Li$_6$1**, Figure 1a). In this study, we examine Li/S full cells with aqueous processed S electrodes cast with **1** vs. **Li$_4$1**, highlighting the importance of pre-lithiation, slurry mixing, and the impact of binder solubility on the self-assembled morphology and final Li/S cell performance.

EXPERIMENTAL SECTION

Synthesis of PBI: PBI **1** was synthesized in a manner similar to that of a reported procedure.[33]

Synthesis of S-GO-CTA nano-composite: The CTAB-modified S−GO nanocomposite (S-GO-CTA) was prepared via a published method[14]. Briefly, 0.58 g of sodium sulfide powder (Alfa Aesar, Na$_2$S, anhydrous) was dissolved in 25 mL of ultrapure water to form a Na$_2$S solution. A sample of 0.72 g of elemental sulfur powder (Alfa Aesar, S, ~325 mesh, 99.5 %) was added to the Na$_2$S solution and stirred with a magnetic stirrer at 60 ˚C until the solution became a transparent orange color (a sodium polysulfide (Na$_2$S$_x$) solution). 18 mL of single layer graphene oxide dispersion (GO, ACS materials, 10 mg/mL) in water was diluted to form a GO suspension (180 mg of GO in 180 mL of ultrapure water). 2.5 mM of cetyltrimethyl ammonium bromide (Sigma Aldrich, CTAB) was added to the GO suspension and stirred for 2 h with a magnetic stirrer. Then the prepared Na$_2$S$_x$ solution was added to the GO-CTAB composite solution and stirred overnight. The as-prepared Na$_2$S$_x$−GO-CTAB composite solution was slowly added to 100 mL of 2.0 M formic acid (Aqua Solutions) and stirred for 2 h to precipitate elemental S onto the GO. Finally, the S−GO-CTA nanocomposite was filtered and washed with acetone and ultrapure water several times to remove salts and impurities. The obtained powder sample was dried at 50 ˚C in a

vacuum oven overnight. The dried powder sample was ground using mortar and pestle and heat-treated in a tube furnace at 155 ˚C for 12 h under an Ar atmosphere.

Material Characterization: The morphology of the powdered samples was observed using a scanning electron microscope (SEM, ZEISS Gemini Ultra 55) at an accelerating voltage of 5.0 kV. Thermogravimetric analysis (TGA, TA Instruments Q5000) was used to determine the content of S in the S-GO-CTA nanocomposite up to 600 ˚C under nitrogen atmosphere. ^{7}Li NMR spectra of LiOH and **Li$_4$1** binder solutions were measured using (AVB-400) spectrometers and the 3.0 M LiCl in D_2O was used as an external reference.

Peel force measurement: **1** and **Li$_4$1** binder were cast onto Al foil and dried in a vacuum chamber overnight at 50 ˚C. The prepared samples were cut into strips 6-mm-wide and 10-mm-long and attached to 3 M adhesive tape. The peel force measurement was conducted with a TCD225 digital force tester (Ametek). The applied load was measured, while the 3M adhesive tape was removed by peeling at an angle of 180˚ at a constant displacement rate of 100 µm/s.

Chemical stability test: The prepared **1** and **Li$_4$1** electrodes were immersed into the electrolyte composed of 1.0 M lithium bis(trifluoromethanesulfonyl)imide (Sigma Aldrich, LiTFSI) in *N*-butyl-*N*-methylpyrrolidinium bis(trifluoromethane sulfonyl)imide (Boulder Ionics, PYR$_{14}$TFSI)/dioxolane (Sigma Aldrich, DOL)/dimethoxyethane (Sigma Aldrich, DME) (1:1:1, *v/v/v*) with 0.50 M lithium nitrate (LiNO$_3$) and the sample was stored in an Ar filled glove-box for 1 month.

Electrochemical tests: The **1** electrode was prepared by mixing the S-GO-CTA nanocomposite, carbon black (Timcal, Super P) with a binder at a weight ratio of 70:22:8 in water. In order to pre-lithiate the PBI binder (**Li$_4$1**), a stoichiometric amount of LiOH was first dissolved in water and the solid mixture of the slurry was added into the LiOH solution. The slurries were stirred using a magnetic stirrer overnight and cast *via* a doctor
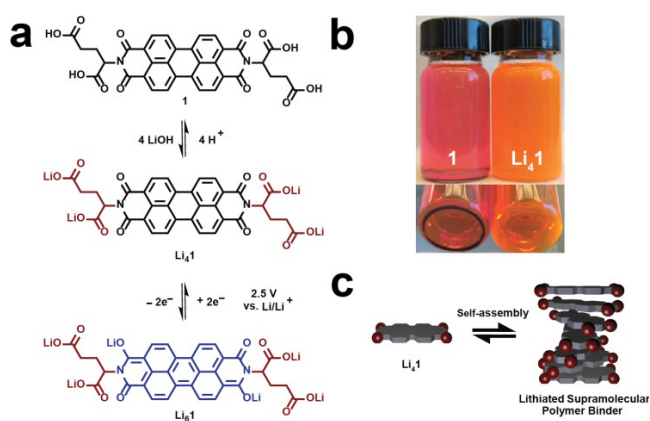
Figure 1. (a) Structure of supramolecular binder PBI **1**, deprotonation to yield water soluble **Li$_4$1**, and *operando* reduction of **Li$_4$1** to **Li$_6$1**. S electrodes with PBI binder were processed from water with either **1** or **Li$_4$1** in this study. During Li/S cell cycling the electroactive PBI core undergoes reversible redox chemistry between **Li$_4$1** and **Li$_6$1** at 2.5 V vs. Li/Li$^+$. (b) Aqueous solubility screens of PBI binders **1** and **Li$_4$1**. (c) Self-assembly of **Li$_4$1** into lithiated supramolecular polymers *via* π-π stacking and intermolecular ion pairing.

blade onto aluminum foil. The electrode was dried at room temperature for 2 hours, and then dried in a vacuum oven at 50 ˚C for 24 hours to fully eliminate residual water. The average S loading of the electrodes was 1.0 mg/cm^2. The electrolyte composed of 1.0 M LiTFSI and 0.50 M LiNO$_3$ in PYR$_{14}$TFSI:DOL:DME (1:1:1, *v/v/v*) was prepared. Type CR2325 coin cells were fabricated with a lithium metal foil as counter/reference electrode, a porous polypropylene separator (2400, Celgard), and 40 µL of electrolyte in a glove box filled with Ar gas. A galvanostatic cycling test of the coin cells was performed using a battery cycler between 1.70–2.80 V at a given C-rate (current). Cyclic voltammetry for the prepared cells was conducted using a potentiostat (Biologic VMP) with a voltage range of 1.70–2.80 V at various scan rates of 0.01, 0.05 and 0.10 mV/s. Rate capability tests were also performed at various discharge C rates from 0.05 C to 3.0 C and then back to 0.20 C. The high S loading **Li$_4$1** electrode (~3.0 mgS/cm^2) was prepared by mixing the S-GO-CTA nanocomposite, carbon black (Timcal, Super P) with a binder at a weight ratio of 72:20:8 in water with a stoichiometric amount of LiOH and casted onto Al foam. The electrode was dried at room temperature for 2 hours, and then dried in a vacuum oven at 50 ˚C for 24

hours to fully eliminate residual water. The same electrode fabrication process was used for the PVDF binder, except the N-methyl-2-pyrrolidone was used as a solvent instead of water. A galvanostatic cycling test of the coin cells was performed using a battery cycler between 1.70–2.60 V at a given C-rate (current) using an electrolyte composed of 1.0 M LiTFSI in DOL:DME (1:1, *v/v*) with 0.50 M $LiNO_3$. Electrolyte to S weight ratio of 8 was kept to compare the
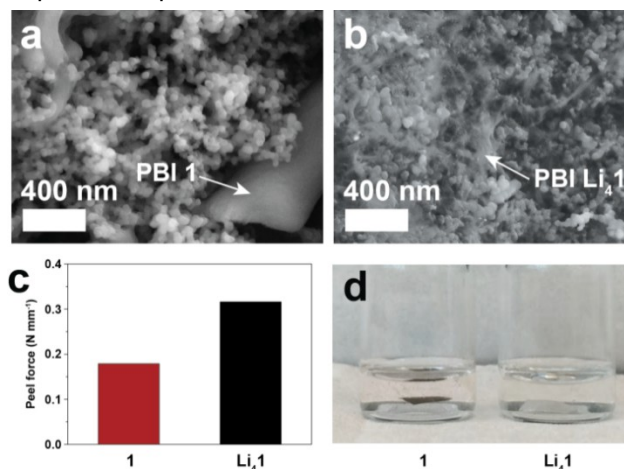
**Figure 2.** SEM images of the S-GO-CTA electrodes prepared with (a) the **1** and (b) the **Li₄1** binders. (c) Peel force measurement results of the **1** and the **Li₄1** binders. (d) The chemical stability test results the **1** and the **Li₄1** electrodes in the organic electrolyte for 1 month. The electrolyte was composed of 1.0 M LiTFSI in PYR₁₄TFSI:DOL:DME (1:1:1 *v/v/v*) with 0.50 M $LiNO_3$.

cell performance between the **Li₄1** and the PVDF electrodes.

Polysulfide absorption test: For the polysulfide absorption test of PBI and PVDF binders, 10 mg of the binder powder was put into the test solution composed of 0.008 M Li_2S_6 in 2 ml of DOL/DME mixture (1:1, *v/v*) overnight.

RESULTS AND DISCUSSION

The molecular design of aqueous-processable PBI binder **1** (Figure 1a) features four carboxylic acid moieties introduced at the imide positions (from glutamic acid) that are lithiated by treatment with LiOH to yield **Li₄1**, a derivative that exhibits excellent solubility in water.[33] Lithiation of the carboxylic acid functional groups was confirmed by ^{7}Li NMR spectroscopy where a distinct resonance is observed at δ 0.09 ppm post lithiation (Figure S1). Notably, **Li₄1** dissolves in water, whereas **1** exhibits poor solubility (Figure 1b). Upon casting S slurries containing **Li₄1**, the aromatic PBI core of **Li₄1** drives self-assembly through π-stacking of the redox-active molecules into supramolecular nanowire architectures, as shown in Figure 1c, that exhibit macromolecular behavior in the electrode common to traditional high-polymer binders like PVDF and PVP. The π-stacking phenomenon of PBI has been extensively studied in both aqueous and non-aqueous environments and shown to yield intricate 1D, 2D, and 3D architectures depending on the subtle interplay of solvation and intermolecular forces.[34-35] Once the PBI binder is assembled into nanowires, cycling of the Li/S cell results in a two-electron reduction of PBI at 2.5 V, further lithiating the binder to **Li₆1** (Figure 1a) as has been
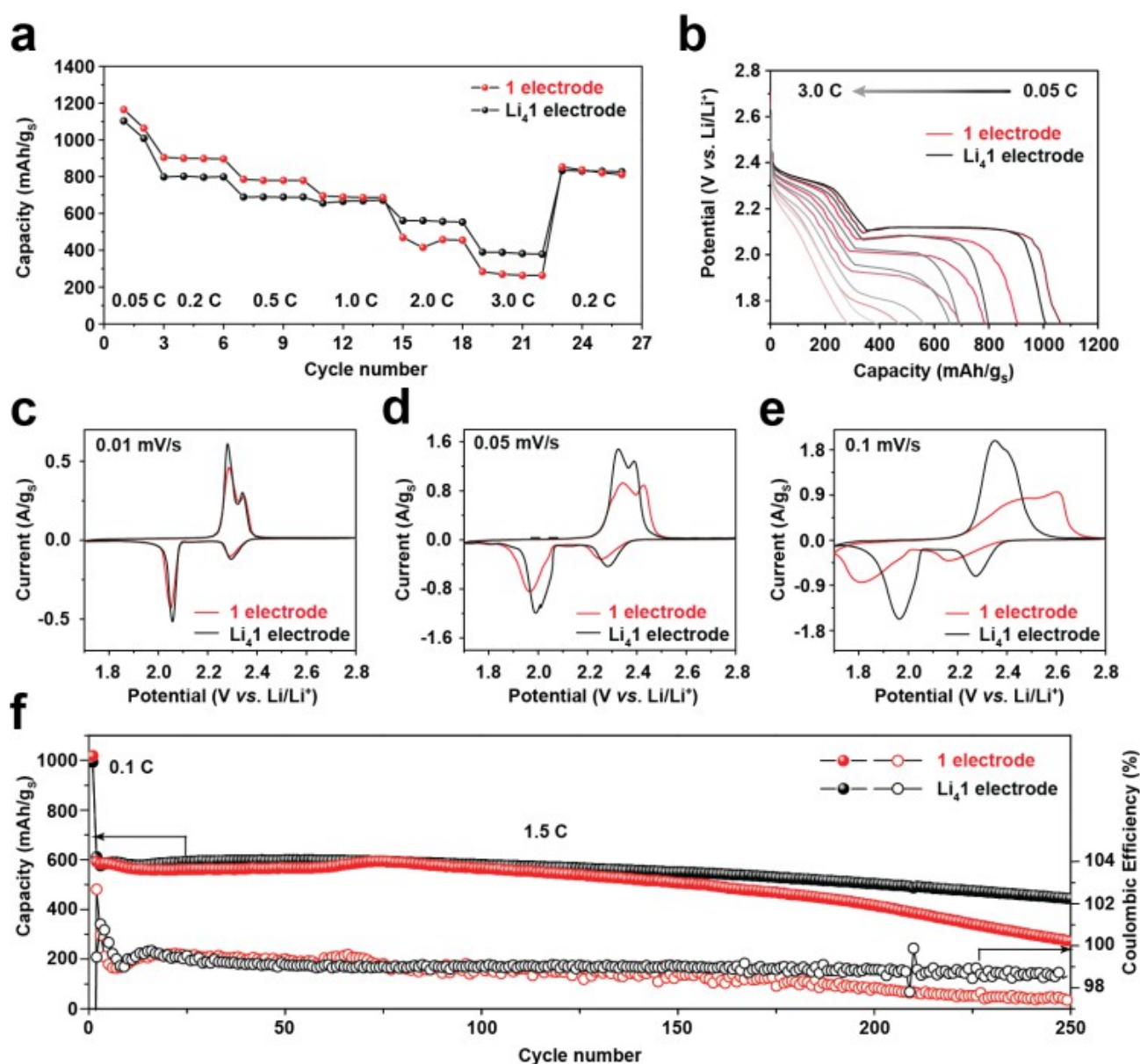
Figure 3. Electrochemical behaviors of **1**-based and **Li₄1**-based electrodes (~1.0 mg S/cm²). (a) Rate capability for **1**-based and **Li₄1**-based electrodes. Charge C-rate was fixed at 0.05 C. (b) Discharge voltage profiles for **1**-based and **Li₄1**-based electrodes. Cyclic voltammograms of **1**-based and **Li₄1**-based electrodes at sweep rates of (c) 0.01 mV/s, (d) 0.05 mV/s and (e) 0.10 mV/s. (f) Cycling performances of **1**-based and **Li₄1**-based electrodes at 1.5C. In all cases, the electrolyte was composed of 1.0 M LiTFSI in PYR₁₄TFSI:DOL:DME (1:1:1 *v/v/v*) with 0.50 M LiNO₃ for all electrochemical tests.

previously observed for PBI redox mediators.[30]

To evaluate the **1** and the **Li₄1** as binder for the S electrode, a cetyltrimethylammonium bromide (CTAB) modified sulfur-graphene oxide (S-GO-CTA) nano-composite (Scanning electron microscope (SEM) image is shown in Figures S2, S content of 78 wt.% was

confirmed by TGA shown in Figure S3) was prepared as active material[14] and mixed with a carbon additive (Super P) and the PBI binders with 70:22:8 weight ratio, respectively, in ultrapure water in order to form a slurry. A stoichiometric amount of LiOH (one for each carboxylic acid of **1**) was added to the slurry to prepare **Li₄1**. The prepared

slurries were cast onto an aluminum (Al) foil current collector. Electrodes prepared using either **1** or **Li₄1** showed similar macroscopic film homogeneity by SEM (Figure S4), indicating that the electrode components are homogeneously distributed. However, the microstructure of **1** and **Li₄1** electrodes are significantly different (Figures 2a and 2b). In electrode **1** (Figure 2a), large bundles of PBI nanowires (~500 nm diameter) corresponding to the morphology of the PBI powder (Figure S5) remained, due to the incomplete dissolution of **1** into water. On the other hand, the **Li₄1** electrode exhibited a unique web-like binder architecture with a wire diameter of 20–30 nm. Increases in interfacial contact between the S-GO nano-composite, Super P nano-particles, and lithiated supramolecular binder are possible by first fully lithiating and dissolving the **Li₄1** then allowing it to self-assemble upon drying the electrode (Figure 2b).

Since the volume expansion of S particles could induce an electronic disconnection between active S particles and the current collector during electrochemical cycling, the adhesion strength of the binder plays an important role in maintaining good electrochemical performance of the S electrode. We anticipated that the web-like PBI nano-architecture of the **Li₄1** electrode would provide stronger physical binding between electrode components and the Al foil current collector. To verify the adhesion properties of the **1** and **Li₄1** binders, peel tests were conducted for the **1** and **Li₄1** films cast onto Al current collectors. As shown in Figure 2c, the **Li₄1** film exhibited approximately 1.8 times higher peel force than that of the **1** film, which indicates that the complete dissolution and reconstruction process of the **Li₄1** nano-architecture can improve the physical stability of the electrode and should result in longer Li/S cell lifetimes. Because the main role of binder in the electrode is physically holding active S and conductive carbon particles onto the current collector, the binder materials need to be chemically compatible with organic electrolytes and insoluble to avoid rapid capacity fade. To verify the chemical stability and insolubility of **1** and **Li₄1**, electrodes cast with each binder were immersed into the electrolyte composed of 1.0 M bis(trifluoromethane)sulfonimide lithium salt (LiTFSI) in 1-butyl-1-methylpyrrolidinium bis(trifluoromethanesulfonyl)imide

(PYR₁₄TFSI):dioxolane (DOL):dimethyoxyethane (DME) (1:1:1, *v/v/v*) with 0.50 M lithium nitrate (LiNO₃) that is used for the electrochemical tests. After one month, no change was observed for electrodes prepared with either **1** or **Li₄1**, indicating that the binders are compatible with the electrolyte (Figure 2d).

Satisfied with the bulk properties of PBI binders, we turned to electrochemical testing of the S-GO-CTA electrodes engineered with binders **1** and **Li₄1**. Type 2325 coin cells were assembled in an Ar-filled glove-box and the rate capabilities of the electrodes were also investigated at various discharge rates of 0.05 C, 0.20 C, 0.50 C, 1.0 C, 2.0 C and 3.0 C (Figures 3a and 3b, 1.0 C = 1675 mA/gS). At 0.05 C, both the **1** and **Li₄1** electrodes showed high specific discharge capacities of about 1165 and 1102 mAh/gS, respectively, however, the specific discharge capacity of the **1** electrode quickly dropped as the discharge C-rate increased, and finally, the discharge capacity reached about 270 mAh/gS at 3.0 C. In contrast, the **Li₄1** electrode successfully retained specific discharge capacities of about 560 and 390 mAh/gS at 2.0 C and 3.0 C discharge rates, respectively, indicating that the pre-lithiated **Li₄1** binder is more suitable for high C-rate applications than binder **1**. It is also notable that the **Li₄1** electrode showed similar or higher operating voltages at all C-rates compared to **1** electrode (Figure 3b). At relatively low C-rates of 0.05 C and 0.50 C, the second plateaus exhibited the same potential for both the **1** and the **Li₄1** electrodes, but the **1** electrode was more severely polarized beginning at 1.0 C and finally, the lower voltage plateau completely disappeared at 3.0 C, whereas that of the **Li₄1** electrode still existed at 3.0 C.

Cyclic voltammetry (CV) was conducted to provide insight into the effect of **1** and **Li₄1** on the electrochemical kinetics of the sulfur electrode. CV scans in the potential range between 1.7 and 2.8 V at the scan rates of 0.01, 0.05 and 0.1 mV/s were informative (Figure 3c-3e). At the sweep rate of 0.01 mV/s, both the **1** and the **Li₄1** electrodes showed two clear oxidation (2.30 and 2.35 V) and reduction peaks (2.30 and 2.06 V) at the same potentials during the charge and discharge processes, respectively; however, the CV peaks of the **1** electrode were significantly broadened and shifted as the

sweep rate increased. In contrast, the redox peaks of the **Li₄1** electrode were sharper and more distinguishable than those of the **1** electrode, even at the high sweep rate of 0.1 mV/s, which means that faster electrochemical processes occur in the **Li₄1** electrode. We hypothesize that the better rate performance of the **Li₄1** electrode is attributed to the networked and conductive nano-architecture of the **Li₄1** (20–30 nm diameter of **Li₄1** wire) that more effectively localizes Li ions near active S particles than the bulk **1** binder structure, resulting in better rate capability of the **Li₄1** electrode. This hypothesis can be supported by the electrochemical impedance spectroscopy test results shown in Figure S6, where the **Li₄1** exhibited smaller cell impedance than that of the **1** electrode.

Galvanostatic cycling performances of the S-GO-CTA electrodes engineered with binders **1** and **Li₄1** at 0.50 C and 1.5 C were evaluated and the results are compared in Figure 3f and Figure S7. As shown in Figure S7a, the **1** and the **Li₄1** electrodes showed similar voltage profiles at the 10th cycle at 0.50 C, however, the **1** electrode exhibited a significant increase of discharge and charge

overpotentials after 150 cycles, whereas the voltage profiles of the **Li₄1** electrode were maintained. At the higher rate of 1.50 C, higher discharge and charge overpotentials for the **1** electrode were present from the 10th cycle compared to those of the **Li₄1** electrode and this deleterious effect became more severe after 250 cycles (Figure S7b). In the cycling test results (Figure S7c), similar discharge specific capacities of 720 mAh/gS and 700 mAh/gS were obtained for the second cycle at 0.50 C, for the **1** and **Li₄1** electrodes, respectively. Then the discharge specific capacity of both electrodes gradually increased, which we attribute to a combination of incomplete wetting of the electrodes by the electrolyte during the early cycles and redistribution of S. After 170 cycles, the **Li₄1** electrode still retained over 85% of the high specific discharge capacity (relative to the specific discharge capacity at the second cycle) while maintaining an excellent Coulombic efficiency of higher than 99%, whereas the electrode incorporating **1** showed a lower capacity retention of about 70% with a Coulombic efficiency of 98%. At 1.5 C (Figure 3f), the **Li₄1** electrode delivered a somewhat higher specific discharge capacity
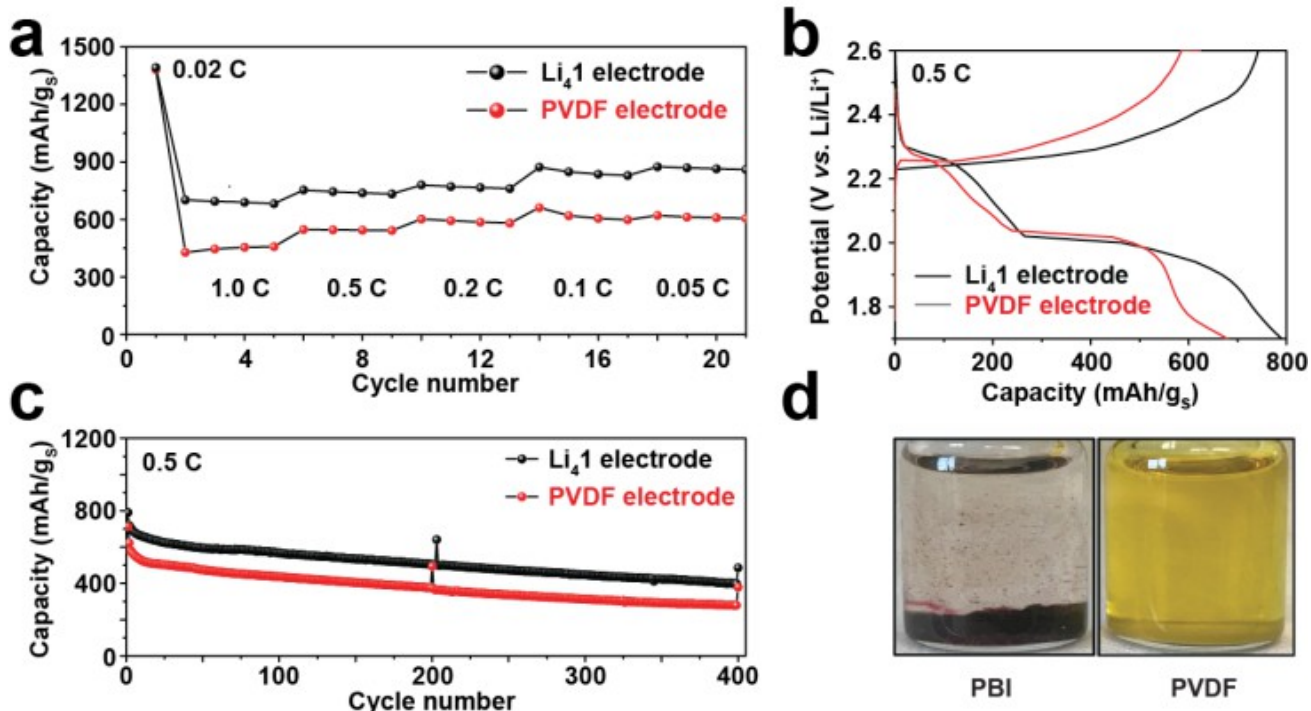
Figure 4. Electrochemical behaviors of high S loading **Li₄1**-based and PVDF electrodes (~3 mg S/cm², Al foam current collector). (a) Rate capability for **Li₄1**-based and PVDF electrodes. Charge C-rate was

fixed at 0.05 C, except the first cycle tested at 0.02 C. (b) Voltage profiles and (c) cycling performances of **Li₄1**-based and PVDF electrodes at 0.5 C (at 0.05 C every 200 cycles). In all cases, the electrolyte was composed of 1.0 M LiTFSI in DOL:DME (1:1 *v/v*) with 0.50 M LiNO₃ for all electrochemical tests. (d) Polysulfide absorption test results.

of 612 mAh/gS compared to that of the **1** (591 mAh/gS) and exhibited good capacity retention of 73% after 250 cycles (~0.11 % of capacity decay per cycle). On the other hand, a specific discharge capacity of only 273 mAh/gS was obtained for the **1** electrode after 250 cycles, which corresponds to a capacity retention of 46% (~0.22 % of capacity decay per cycle). The favorable cycle-life of the **Li₄1** electrode can be explained by the better adhesion strength of the **Li₄1** binder, according to the peel force measurement test (since the S undergoes a volume expansion/contraction (~76%) during electrochemical cycling).

Morphological changes of electrodes after electrochemical cycling reflect how well a binder maintains the integrity of the electrode under stress. Therefore, we studied electrodes fabricated with **1** and **Li₄1** binders by SEM after 250 cycles at 1.5 C. As shown in Figure S8, significant cracking was observed for the cycled **1** electrode (Figure S8a), whereas the **Li₄1** electrode maintained a morphology similar to its pristine pre-cycled appearance (Figure S8b). The volume change that occurred during cycling resulted in significant cracking because of the relatively weak adhesion strength of binder **1**. As a result, the active S particles may lose electrical contact with the current collector. This observation helps to rationalize the accelerated capacity fade and reduced Coulombic efficiency experienced by electrode **1** compared to electrode **Li₄1**.

Since high areal S loading is essential to developing practical Li/S cells, it is worthwhile to demonstrate the suitability of the **Li₄1** binder for higher S loading electrodes. An Al foam current collector that is suitable for increasing the S mass loading and S content of the electrode, while the maintaining good cell performances[18] was used to prepare the high S loading **Li₄1** and PVDF electrodes (S loading: ~ 3.0 mg/cm², S Content: 64 %). As shown in the rate capability test results (Figure 4a), both the **Li₄1** and PVDF electrodes exhibited very high specific discharge capacity of 1380–1390 mAh/gS at 0.02 C, however, the **Li₄1** electrode exhibited 1.3-1.6 times higher specific discharge capacity than

that of PVDF electrode, once the test discharge C-rate increased to 1.0-0.05 C.

The long-term cycling performance of the **Li₄1** and PVDF electrodes were also demonstrated at 0.50 C for 400 cycles (cycled at 0.05 C every 200 cycles) and the results are shown in Figure 4b and 4c. The voltage profiles of the **Li₄1** and PVDF electrodes at 0.50 C for the first cycle (Figure 4b) clearly show the different discharge behaviors, where the second discharge plateau of the **Li₄1** electrode is relatively prolonged compared to that of the PVDF electrode, resulting in the higher specific discharge capacity of the **Li₄1** electrode (790 mAh/gS vs. 713 mAh/gS for the PVDF electrode). This can be attributed to the good chemical affinity of the PBI binder for the lithium polysulfide in the electrolyte, which helps to secure the lithium polysulfides near the surface of the S electrode. So more lithium polysulfide dissolved from the S electrode during the discharge process can be re-deposited, which is reflected in the prolonged second discharge plateau of the **Li₄1** electrode compared to that of the PVDF electrode. Good chemical affinity of the PBI binder to the lithium polysulfide was confirmed by the polysulfide absorption test shown in Figure 4d. The orange color of the test solution that indicates the existence of lithium polysulfides became colorless for the PBI binder, which means that the lithium polysulfides in the test solution were chemically absorbed/adsorbed by the PBI binder powder. In contrast, the color of the test solution for the PVDF binder did not change, indicating no significant chemical affinity of the PVDF binder to lithium polysulfide. During 400 cycles (Figure 4c), the **Li₄1** electrode exhibited 1.4 times higher specific discharge capacity (in an average, ~ 0.10 % of capacity decay per cycle) than that of the PVDF electrode (~ 0.14 % of capacity decay per cycle) and the specific capacity of about 500 mAh/gS was still obtained after 400 cycles at 0.05 C, which verifies that the **Li₄1** binder is suitable for high S loading electrodes.

In summary, renewed vigor in electrifying the transportation sector has translated directly into demand for rapid battery

innovation. Binder optimization is critical to advanced S electrode development for successful commercialization. Here, we have demonstrated a binder concept based on self-assembled PBI nanowires that both enhance the performance of the S electrode as well as the manufacturability by moving from toxic organic solvents to water. The results of the galvanostatic and the potentiostatic tests for the **1** and the **Li$_4$1** electrodes show that the pre-lithiation process of the PBI binder improved not only the cyclability, but also the high rate capability of the cells. The high S loading (~3.0 mgS/cm^2) **Li$_4$1** electrodes showed better high rate performance and 1.4 times higher specific discharge capacity during 400 cycles at 0.50 C than that of the PVDF electrode. Translating supramolecular chemistry concepts into battery electrode design has proven to be valuable for processing S electrodes, and redox-mediating binders like **Li$_4$1** offer opportunities to enhance the high rate and lifetime performance of next-generation S-based electrodes.

ASSOCIATED CONTENT

Supporting Information

Supporting Figures S1–S8. This material is available free of charge via the Internet at http://pubs.acs.org.

AUTHOR INFORMATION

Corresponding Author

* bahelms@lbl.gov and ejcairns@lbl.gov

REFERENCES

1. Bruce, P. G.; Freunberger, S. A.; Hardwick, L. J.; Tarascon, J.-M., Li-O2 and Li-S batteries with high energy storage. *Nat. Mater.* **2012,** *11* (1), 19-29.
2. Ji, X.; Nazar, L. F., Advances in Li-S batteries. *J. Mater. Chem.* **2010,** *20* (44), 9821-9826.
3. Yang, Y.; Zheng, G.; Cui, Y., Nanostructured sulfur cathodes. *Chem. Soc. Rev.* **2013,** *42* (7), 3018-3032.
4. Manthiram, A.; Fu, Y.; Chung, S.-H.; Zu, C.; Su, Y.-S., Rechargeable Lithium–Sulfur Batteries. *Chem. Rev.* **2014,** *114* (23), 11751-11787.
5. Mikhaylik, Y. V.; Akridge, J. R., Polysulfide Shuttle Study in the Li/S Battery System. *J. Electrochem. Soc.* **2004,** *151* (11), A1969-A1976.
6. Yamin, H.; Peled, E., Electrochemistry of a nonaqueous lithium/sulfur cell. *J. Power Sources* **1983,** 9 (3), 281-287.
7. Zheng, G.; Zhang, Q.; Cha, J. J.; Yang, Y.; Li, W.; Seh, Z. W.; Cui, Y., Amphiphilic Surface Modification of Hollow Carbon Nanofibers for Improved Cycle Life of Lithium Sulfur Batteries. *Nano Lett.* **2013,** *13* (3), 1265-1270.
8. Ji, X.; Lee, K. T.; Nazar, L. F., A highly ordered nanostructured carbon-sulphur cathode for lithium-sulphur batteries. *Nat. Mater.* **2009,** *8* (6), 500-506.
9. Ji, L.; Rao, M.; Zheng, H.; Zhang, L.; Li, Y.; Duan, W.; Guo, J.; Cairns, E. J.; Zhang, Y., Graphene Oxide as a Sulfur Immobilizer in High Performance Lithium/Sulfur Cells. *J. Am. Chem. Soc.* **2011,** *133* (46), 18522-18525.
10. Hwa, Y.; Zhao, J.; Cairns, E. J., Lithium Sulfide (Li2S)/Graphene Oxide Nanospheres with Conformal Carbon Coating as a High-Rate, Long-Life Cathode for Li/S Cells. *Nano Lett.* **2015,** *15* (5), 3479-3486.
11. Song, J.; Gordin, M. L.; Xu, T.; Chen, S.; Yu, Z.; Sohn, H.; Lu, J.; Ren, Y.; Duan, Y.; Wang, D., Strong Lithium Polysulfide Chemisorption on Electroactive Sites of Nitrogen-Doped Carbon Composites For High-Performance Lithium–Sulfur Battery Cathodes. *Angew. Chem. Int. Ed.* **2015,** *54* (14), 4325-4329.
12. Tang, C.; Zhang, Q.; Zhao, M.-Q.; Huang, J.-Q.; Cheng, X.-B.; Tian, G.-L.; Peng, H.-J.; Wei, F., Nitrogen-Doped Aligned Carbon Nanotube/Graphene Sandwiches: Facile Catalytic Growth on Bifunctional Natural Catalysts and Their Applications as Scaffolds for High-Rate Lithium-Sulfur Batteries. *Adv. Mater.* **2014,** *26* (35), 6100-6105.
13. Jozwiuk, A.; Sommer, H.; Janek, J.; Brezesinski, T., Fair performance comparison of different carbon blacks in lithium–sulfur batteries with practical mass loadings – Simple design competes with complex cathode architecture. *J. Power Sources* **2015,** *296*, 454-461.
14. Song, M.-K.; Zhang, Y.; Cairns, E. J., A Long-Life, High-Rate Lithium/Sulfur Cell: A Multifaceted Approach to Enhancing Cell Performance. *Nano Lett.* **2013,** *13* (12), 5891-5899.
15. Li, Z.; Jiang, Y.; Yuan, L.; Yi, Z.; Wu, C.; Liu, Y.; Strasser, P.; Huang, Y., A Highly Ordered Meso@Microporous Carbon-Supported

Sulfur@Smaller Sulfur Core–Shell Structured Cathode for Li–S Batteries. *ACS Nano* **2014,** *8* (9), 9295-9303.

16. Demir-Cakan, R.; Morcrette, M.; Nouar, F.; Davoisne, C.; Devic, T.; Gonbeau, D.; Dominko, R.; Serre, C.; Férey, G.; Tarascon, J.-M., Cathode Composites for Li–S Batteries via the Use of Oxygenated Porous Architectures. *J. Am. Chem. Soc.* **2011,** *133* (40), 16154-16160.

17. Chen, R.; Zhao, T.; Lu, J.; Wu, F.; Li, L.; Chen, J.; Tan, G.; Ye, Y.; Amine, K., Graphene-Based Three-Dimensional Hierarchical Sandwich-type Architecture for High-Performance Li/S Batteries. *Nano Lett.* **2013,** *13* (10), 4642-4649.

18. Hwa, Y.; Seo, H. K.; Yuk, J.-M.; Cairns, E. J., Freeze-Dried Sulfur-Graphene Oxide-Carbon Nanotube Nanocomposite for High Sulfur-Loading Lithium/Sulfur Cells. *Nano Lett.* **2017,** *17* (11), 7086-7094.

19. Li, C.; Ward, A. L.; Doris, S. E.; Pascal, T. A.; Prendergast, D.; Helms, B. A., Polysulfide-Blocking Microporous Polymer Membrane Tailored for Hybrid Li-Sulfur Flow Batteries. *Nano Lett.* **2015,** *15* (9), 5724-5729.

20. Su, Y.-S.; Manthiram, A., Lithium–sulphur batteries with a microporous carbon paper as a bifunctional interlayer. *Nat. Commun.* **2012,** *3*, 1166.

21. Ward, A. L.; Doris, S. E.; Li, L.; Hughes, M. A.; Qu, X.; Persson, K. A.; Helms, B. A., Materials Genomics Screens for Adaptive Ion Transport Behavior by Redox-Switchable Microporous Polymer Membranes in Lithium–Sulfur Batteries. *ACS Cent. Sci.* **2017,** *3* (5), 399-406.

22. Agostini, M.; Xiong, S.; Matic, A.; Hassoun, J., Polysulfide-containing Glyme-based Electrolytes for Lithium Sulfur Battery. *Chem. Mater.* **2015,** *27* (13), 4604-4611.

23. Zhang, S.; Ueno, K.; Dokko, K.; Watanabe, M., Recent Advances in Electrolytes for Lithium–Sulfur Batteries. *Adv. Energy Mater.* **2015,** *5* (16), 1500117.

24. Marmorstein, D.; Yu, T. H.; Striebel, K. A.; McLarnon, F. R.; Hou, J.; Cairns, E. J., Electrochemical performance of lithium/sulfur cells with three different polymer electrolytes. *J. Power Sources* **2000,** *89* (2), 219-226.

25. Basile, A.; Bhatt, A. I.; O'Mullane, A. P., Stabilizing lithium metal using ionic liquids for long-lived batteries. *Nat. Commun.* **2016,** *7*, ncomms11794.

26. Choi, N.-S.; Chen, Z.; Freunberger, S. A.; Ji, X.; Sun, Y.-K.; Amine, K.; Yushin, G.; Nazar, L. F.; Cho, J.; Bruce, P. G., Challenges Facing Lithium Batteries and Electrical Double-Layer Capacitors. *Angew. Chem. Int. Ed.* **2012,** *51* (40), 9994-10024.

27. Frischmann, P. D.; Hwa, Y.; Cairns, E. J.; Helms, B. A., Redox-Active Supramolecular Polymer Binders for Lithium–Sulfur Batteries That Adapt Their Transport Properties in Operando. *Chem. Mat.* **2016,** *28* (20), 7414-7421.

28. Wurthner, F., Perylene bisimide dyes as versatile building blocks for functional supramolecular architectures. *Chem. Commun.* **2004,** (14), 1564-1579.

29. Kolosnitsyn, V.; Karaseva, E., Lithium-sulphur battery with high specific energy. Google Patents: 2014.

30. Frischmann, P. D.; Gerber, L. C. H.; Doris, S. E.; Tsai, E. Y.; Fan, F. Y.; Qu, X.; Jain, A.; Persson, K. A.; Chiang, Y.-M.; Helms, B. A., Supramolecular Perylene Bisimide-Polysulfide Gel Networks as Nanostructured Redox Mediators in Dissolved Polysulfide Lithium–Sulfur Batteries. *Chem. Mat.* **2015,** *27* (19), 6765-6770.

31. Meini, S.; Elazari, R.; Rosenman, A.; Garsuch, A.; Aurbach, D., The Use of Redox Mediators for Enhancing Utilization of Li2S Cathodes for Advanced Li–S Battery Systems. *J. Phys. Chem. Lett.* **2014,** *5* (5), 915-918.

32. Rosenman, A.; Markevich, E.; Salitra, G.; Aurbach, D.; Garsuch, A.; Chesneau, F. F., Review on Li-Sulfur Battery Systems: an Integral Perspective. *Adv. Energy Mater.* **2015,** *5* (16), 1500212.

33. Araujo, R. F.; Silva, C. J. R.; Paiva, M. C.; Franco, M. M.; Proenca, M. F., Efficient dispersion of multi-walled carbon nanotubes in aqueous solution by non-covalent interaction with perylene bisimides. *RSC Adv.* **2013,** *3* (46), 24535-24542.

34. Chen, Z.; Lohr, A.; Saha-Moller, C. R.; Wurthner, F., Self-assembled [small pi]-stacks of functional dyes in solution: structural and thermodynamic features. *Chem. Soc. Rev.* **2009,** *38* (2), 564-584.

35. Görl, D.; Zhang, X.; Würthner, F., Molecular Assemblies of Perylene Bisimide Dyes in Water. *Angew. Chem. Int. Ed.* **2012,** *51* (26), 6328-6348.

Water-Processable Supramolecular Binder

Li$_4$1   Self-assembly

PBI Li$_4$1